CONDITIONING DISCRETE FRACTURE NETWORK MODELS OF GROUNDWATER FLOW

K. CLIFFE, D. HOLTON, P. HOUSTON, C. JACKSON, S. JOYCE, AND A. MILNE

Abstract. Many geological formations consist of crystalline rock that have very low matrix permeability but allow flow through an interconnected network of fractures. Understanding the flow of groundwater through such rocks is important in considering disposal of radioactive waste in underground repositories. A specific area of interest is the conditioning of fracture transmissivities on measured values of pressure in these formations. While there are existing methods to condition transmissivity fields on transmissivity, pressure and flow measurements for a continuous porous medium, considerably less work has been devoted to conditioning discrete fracture networks. This article presents two new methods for conditioning fracture transmissivities on measured pressures in a discrete fracture network. The first approach adopts a linear approximation when fracture transmissivities are mildly heterogeneous, while the minimisation of a suitable objective function is undertaken when fracture transmissivities are highly heterogeneous. The second conditioning algorithm is a Bayesian method that finds a maximum a posteriori (MAP) estimator which maximises the posterior distribution defined by Bayes' theorem using information from the prior distribution of fracture transmissivities and observations in the form of measured pressures. The conditioning methods are tested on two separate, large scale test cases that model a potential site for radioactive waste disposal. Results from these test cases are shown and comparisons between the two conditioning methods are made.

Key Words. Conditioning, Groundwater Flow, Discrete Fracture Network, Finite Element Methods.

1. Introduction

Many geological formations consist of crystalline rock that have very low matrix permeability but allow flow through an interconnected network of fractures. Understanding the flow of groundwater through such rocks is important in considering disposal of radioactive waste in underground repositories. In our work it is assumed that there is no interaction between groundwater flow (and the pollutants it may carry) in the fractures and the surrounding rock matrix; this setting is known as a discrete fracture network (DFN). A DFN is characterised by the properties of the fractures, namely, the density of the fractures, their size, orientation and transmissivity. The transmissivity of a fracture is defined as the rate of groundwater flow per unit pressure gradient. It thus gives a measure of the ease with which groundwater can pass through a material (a fracture in our case). In our work the fractures are modelled such that the fracture walls are represented as two parallel plates with

groundwater flowing between them. In this setting, the fracture transmissivity is proportional to the cube of the fracture aperture (width between the fracture walls) [21], and both the aperture and transmissivity are constant over the fracture. In a problem of practical relevance, there are generally too many fractures for all of their properties to be measured. To remedy this problem when numerically modelling a DFN, a stochastic approach can be exploited; here distributions of fracture properties (aperture, length, orientation, location) are inferred from field measurements and are subject to uncertainty [12, 17]. Realisations of fractures can be generated in a given domain with fracture properties (aperture, length, orientation, location) sampled from distributions consistent with observed measurements. Fractures with known properties can also be included deterministically in a model of this type. This paper develops two numerical methods in a DFN setting to condition fracture transmissivities on measured values of the pressure available from test site data. The groundwater flow equation [1] can be used to calculate the pressure in a fracture. DFNs are modelled numerically with suitable boundary conditions at both fracture intersections and the domain boundaries [8]. Our work exploits a finite element approach to modelling groundwater flow in a DFN. Alternative numerical methods for solving flow in a DFN are discussed in Jing [10].

The problem considered in this article can be summarised in a continuous setting (before discretisation of the domain) as follows: determine $\mathbf{T}$ such that

$$\|P(\mathbf{X}_M) - \mathbf{P}_M\| = \min!,$$

under the constraint,

$$\nabla \cdot (\mathbf{T}\nabla P) = 0 \text{ in } \Omega,$$

subject to appropriate boundary conditions. Here, $\mathbf{T}$ is a vector of fracture transmissivities (containing hundreds or thousands of fracture transmissivities), $\mathbf{P}_M$, $M \geq 1$, is a vector of measured pressures that are to be matched, $\mathbf{X}_M$, $M \geq 1$, denotes the locations of the measurement points, P is the pressure, Ω is the domain of the fracture network and $\|\cdot\|$ denotes an appropriate norm. Boundary conditions are imposed both on the boundaries of the problem domain Ω, as well as at fracture intersections. Generally, there are far less pressure measurements than fracture transmissivities.

When studying DFNs it is common to use more than one realisation of the DFN due to uncertainties in the fracture properties. In this setting, the geometry of the fractures is sampled from various distributions; thus each realisation will have different fracture geometry. Calibration is the process of modifying input parameters to a model until the output from the model matches observed data. Each realisation should be calibrated using as much available data as possible. In our work the model parameters are the fracture transmissivities and they are conditioned on measured pressures.

While there are existing methods to condition transmissivity fields on transmissivity, pressure and flow measurements for a continuous porous medium [9, 19, 20], there is considerably less work within the literature on conditioning DFNs. An exception is the recent work by Frampton and Cvetkovic [5] who condition the parameters of a fracture transmissivity distribution in a DFN setting, but they do not condition fracture transmissivities directly. Conditioning fracture transmissivities on pressure or flow values is a complex problem because the measured pressures are dependent on all the fracture transmissivities in the DFN.

In this article, we present two new methods for conditioning fracture transmissivities in a DFN on measured pressure values. Both methods consider one realisation,

where the geometry of the DFN is assumed fixed. In particular, only fracture transmissivities are adjusted to fit measured pressures, while keeping the position and orientation of each fracture fixed. The first method adopts a linear approximation when fracture transmissivities are mildly heterogeneous and generalises this approach to the minimisation of an appropriate objective function when fracture transmissivities are highly heterogeneous. This method is based on a generalisation of previous work undertaken on conditioning transmissivity values in a continuous porous medium [3] and shares some of the techniques used in inverse problems in hydrology for a continuous porous medium [9, 14, 15, 19, 20].

The second method we develop is a Bayesian conditioning method similar to the work developed in a continuous porous medium setting in the articles [2, 11]. Stuart [18] gives a concise review of the Bayesian setting used in inverse methods for PDEs. Here, Bayes' theorem is used to give an expression of proportionality for the posterior distribution of fracture log transmissivities in terms of the prior distribution and the data available through pressure measurements. The fracture transmissivities are assumed to be normally distributed with a given mean and covariance, and the measured pressures are assumed to be normally distributed values, each with a given error. From the expression of proportionality for the posterior distribution of fracture transmissivities, the modes of the posterior distribution (the points of highest likelihood for the fracture transmissivities given the measured pressures) are computed numerically.

The paper is structured as follows. In Section 2 we introduce the PDE model used to determine the pressure in a fracture network, together with details of the application of the finite element method to the DFN. Section 3 introduces the two conditioning methods, while section 4 describes the two test cases that will be considered in this article. Results obtained from both the conditioning methods are presented in section 5. Here, both algorithms are implemented in the existing finite element code ConnectFlow [8] developed and marketed by Serco, which numerically models groundwater flow in a DFN using a finite element approach. Finally, we summarise the work presented in this article and draw some conclusions in Section 6.

2. Finite Element Treatment of Intersecting Fractures

In this section we outline the finite element (FE) method implemented within ConnectFlow to discretise a DFN in order to compute the residual pressure on fracture intersections. The FE method employed here is based on a standard FE discretisation of each fracture, together with a static condensation technique which eliminates the internal degrees of freedom on each fracture, thereby leading to a global system of equations for the unknowns defined on the fracture intersections only. In order to present this algorithm in the simplest possible setting, here we shall confine ourselves to the case of two intersecting fractures. The extension of the FE method to a large scale DFN follows analogously; for further details, we refer to Milne [13] and Hartley [8]. With this in mind, we assume that the problem domain $\Omega \subset \mathbb{R}^3$ is partitioned into two two–dimensional planes f_1 and f_2 (which represent the fractures) with boundaries ∂f_1 and ∂f_2, respectively. Here, we assume that the fractures f_1 and f_2 do not overlap, in the sense that their orientations in $\mathbb{R}^3$ are not identical, but that the fractures do intersect one another along a one–dimensional line $\Gamma := f_1 \cap f_2$. The residual pressure

$$(1) \qquad\qquad P = P_G + \rho g\,(z - z_0)\,,$$

is to be calculated across f_1 and f_2, where P_G is the groundwater pressure, ρ is the groundwater density, g is gravitational acceleration, z is the elevation and z_0

is a reference elevation. Defining $\tilde{T}_f = T_f/(\rho g)$, the steady state groundwater flow equation is given by: find P such that

$$(2) \qquad \nabla \cdot \left(\tilde{T}_{f_i} \nabla P \right) = 0, \text{ in } f_i, \ i = 1, 2,$$

$$(3) \qquad P = P_D, \text{ on } \partial f_i, \ i = 1, 2,$$

where the transmissivities $\tilde{T}_{f_1}$ and $\tilde{T}_{f_2}$ are assumed constant on f_1 and f_2, respectively, and ∇ denotes the two dimensional gradient operator. At the fracture intersection Γ, the following conditions hold:

(1) The groundwater pressure is continuous between intersecting fractures; i.e., $P|_{f_1 \cap \Gamma} = P|_{f_2 \cap \Gamma}$.

(2) Groundwater is conserved at the intersection, so that groundwater which flows out of one fracture flows into the other fracture and there is no build up of groundwater at the intersection. In the continuous setting, this is written as $Q_{f_1} := T_{f_1} \nabla P_{f_1} = Q_{f_2} := T_{f_2} \nabla P_{f_2}$, where Q_{f_1} and Q_{f_2} are the flows coming from f_1 and f_2, respectively, and P_{f_1} and P_{f_2} are the pressures defined on f_1 and f_2, respectively.

We now outline the FE method employed to discretise (2), (3), together with the above intersection conditions. To this end, we assume that the fractures f_i, $i = 1, 2$, can be subdivided into shape-regular meshes $\mathcal{T}_{f_i} = \{\kappa_{f_i}\}$, $i = 1, 2$, respectively, consisting of triangular elements κ_{f_i}, $i = 1, 2$. Moreover, we define N_{f_i}, $i = 1, 2$, to denote the set of vertices contained in the meshes $\mathcal{T}_{f_i} = \{\kappa_{f_i}\}$, $i = 1, 2$, respectively. In the following, we shall refer to these sets as the sets of so–called *local nodes*. Further, we write n_{f_i} to denote the cardinality of N_{f_i}, $i = 1, 2$.

The fracture intersection Γ is subdivided into a set N_Γ of so–called *global nodes*; here, we write n_Γ to denote the cardinality of the set N_Γ. For simplicity of presentation, we assume that each global node contained in the set N_Γ corresponds to a local node on f_1 and f_2. That is, we may define the set of global nodes as $N_\Gamma := N_{f_1} \cap N_{f_2}$. In general, this condition is rather restrictive, since it requires $\mathcal{T}_{f_1}$ and $\mathcal{T}_{f_2}$ to match on Γ. We emphasise that this constraint is only imposed for simplicity of presentation; for the case of the more general setting, see [13]. With this notation, we introduce the finite element spaces

$$V_{f_i} = \{v \in H_0^1(f_i) : v|_{\kappa_{f_i}} \in \mathcal{P}^1(\kappa_{f_i}), \kappa_{f_i} \in \mathcal{T}_{f_i}\}, \qquad i = 1, 2,$$

where $\mathcal{P}^1(\kappa_{f_i})$ denotes the set of linear polynomials on κ_{f_i}, $i = 1, 2$.

For each global node I, $I = 1, ..., n_\Gamma$, a corresponding global basis function Ψ_I is calculated over the problem domain Ω. With this in mind, we denote $\Psi_I^{f_i}$, $i = 1, 2$, to be the restriction of Ψ_I over f_i, $i = 1, 2$, respectively, such that $\Psi_I = \Psi_I^{f_1} + \Psi_I^{f_2}$, where $\Psi_I^{f_i} \in V_{f_i}$, $i = 1, 2$.

On each fracture, Ψ_I is calculated as the FE solution to the steady state groundwater flow equation (2) with P replaced by Ψ_I, subject to the boundary conditions: $\Psi_I = 1$ at global node I and $\Psi_I = 0$, otherwise. Therefore, the contributions $\Psi_I^{f_1}$ and $\Psi_I^{f_2}$ to the global basis function Ψ_I corresponding to the global node I are calculated by solving the linear systems: find $\Psi_I^{f_i} \in V_{f_i}$, $i = 1, 2$, such that

$$(4) \qquad \int_{f_i} \tilde{T}_{f_i} \nabla \Psi_I^{f_i} \cdot \nabla v^{f_i} dx = 0 \qquad \forall v^{f_i} \in V_{f_i},$$

subject to the boundary conditions: $\Psi_I^{f_i} = 1$, $i = 1, 2$, at global node I and $\Psi_I^{f_i} = 0$, $i = 1, 2$, at all other global nodes on Γ.

The FE space V_Γ consisting of the global basis functions may now be defined as

$$V_\Gamma = \text{span} \{\Psi_I\}_{I=1}^{n_\Gamma}.$$

In order to take into account the Dirichlet boundary conditions, it is necessary to calculate a (boundary) contribution $\Psi_{I,D}$ to the global basis function Ψ_I, $I = 1, \ldots, n_\Gamma$. To this end, we define the contributions $\Psi_{I,D}^{f_1}$ on f_1 and $\Psi_{I,D}^{f_2}$ on f_2 to $\Psi_{I,D}$ as follows: find $\Psi_{I,D}^{f_i} \in P_D + V_{f_i}$, $i = 1, 2$, such that

$$(5) \qquad \int_{f_i} \tilde{T}_{f_i} \nabla \Psi_{I,D}^{f_i} \cdot \nabla v^{f_i} dx = 0 \qquad \forall v^{f_i} \in V_{f_i},$$

subject to the (additional) boundary condition $\Psi_{I,D}^{f_i} = 0$ on Γ, $i = 1, 2$.

The flow Q_I at a global node I, $I = 1, ..., n_\Gamma$, from a fracture $f = f_1, f_2$, is calculated as follows:

$$(6) \qquad Q_I = \int_f \nabla \Psi_I \cdot \left(\tilde{T}_f \nabla P_h\right) dx \qquad \forall \Psi_I \in V_\Gamma,$$

where P_h is defined by

$$(7) \qquad P_h = \sum_{J=1}^{n_\Gamma} \left(\Psi_{J,D} + \Psi_J P_{\Gamma_J}\right).$$

Here, P_{Γ_J} denotes the value of the pressure at the Jth global node. The pressure P_Γ at the fracture intersection Γ can now be calculated by enforcing the condition that flow is conserved at the fracture intersection. Thereby, employing (6), we deduce that

$$(8) \qquad \int_{f_1} \nabla \Psi_I^{f_1} \cdot \left(\tilde{T}_{f_1} \nabla P_h\right) dx + \int_{f_2} \nabla \Psi_I^{f_2} \cdot \left(\tilde{T}_{f_2} \nabla P_h\right) dx = 0, \qquad I = 1, ..., n_\Gamma.$$

Inserting (7) into (8) gives

$$(9) \qquad \begin{aligned} &\sum_{J=1}^{n_\Gamma} \left(\tilde{T}_{f_1} \int_{f_1} \nabla \Psi_I^{f_1} \cdot \nabla \Psi_{J,D}^{f_1} dx + \tilde{T}_{f_1} P_{\Gamma_J} \int_{f_1} \nabla \Psi_I^{f_1} \cdot \nabla \Psi_J^{f_1} dx\right) + \\ &\sum_{J=1}^{n_\Gamma} \left(\tilde{T}_{f_2} \int_{f_2} \nabla \Psi_I^{f_2} \cdot \nabla \Psi_{J,D}^{f_2} dx + \tilde{T}_{f_2} P_{\Gamma_J} \int_{f_2} \nabla \Psi_I^{f_2} \cdot \nabla \Psi_J^{f_2} dx\right) = 0, \end{aligned}$$

for $I = 1, ..., n_\Gamma$. Introducing the notation

$$(10) \qquad A_{IJ} = \tilde{T}_{f_1} \int_{f_1} \nabla \Psi_I^{f_1} \cdot \nabla \Psi_J^{f_1} dx + \tilde{T}_{f_2} \int_{f_2} \nabla \Psi_I^{f_2} \cdot \nabla \Psi_J^{f_2} dx$$

for $I, J = 1, ..., n_\Gamma$, and

$$(11) \qquad B_I = -\tilde{T}_{f_1} \sum_{J=1}^{n_\Gamma} \int_{f_1} \nabla \Psi_I^{f_1} \cdot \nabla \Psi_{J,D}^{f_1} dx - \tilde{T}_{f_2} \sum_{J=1}^{n_\Gamma} \int_{f_2} \nabla \Psi_I^{f_2} \cdot \nabla \Psi_{J,D}^{f_2} dx,$$

for $I = 1, ..., n_\Gamma$, the matrix system corresponding to (9) may be written in the following form

$$(12) \qquad \begin{pmatrix} A_{11} & \cdots & A_{n_\Gamma 1} \\ \cdots & \cdots & \cdots \\ A_{1 n_\Gamma} & \cdots & A_{n_\Gamma n_\Gamma} \end{pmatrix} \begin{pmatrix} P_{\Gamma_1} \\ \cdots \\ P_{\Gamma_{n_\Gamma}} \end{pmatrix} = \begin{pmatrix} B_1 \\ \cdots \\ B_{n_\Gamma} \end{pmatrix}.$$

The matrix system (12) may now be inverted in order to compute P_Γ; thereby, substituting P_Γ into (7), the pressure over the two fractures f_1 and f_2 can subsequently be calculated. The overall computational implementation is now summarised in Algorithm 2.1 below.

Algorithm 2.1. *FE method on a DFN.*

(1) *Construct finite element meshes $\mathcal{T}_{f_i} = \{\kappa_{f_i}\}$, $i = 1, 2$, over each fracture f_i, $i = 1, 2$, in the DFN, respectively.*

(2) *Discretise the fracture intersection Γ into n_Γ global nodes belonging to the set N_Γ, such that $N_\Gamma = N_{f_1} \cap N_{f_2}$.*

(3) *DO $I = 1, 2, \ldots, n_\Gamma$*
   Compute $\Psi_I^{f_i}$ and $\Psi_{I,D}^{f_i}$ using (4) and (5), respectively, $i = 1, 2$.
   END DO

(4) *Calculate A_{IJ} and B_J defined in (10) and (11), respectively, $I, J = 1, \ldots, n_\Gamma$.*

(5) *Calculate $P_{\Gamma_I}, I = 1, .., n_\Gamma$, by solving the matrix system (12).*

(6) *Calculate the pressure across the fracture network using the approximation $P_h = \sum_{J=1}^{n_\Gamma} \left(\Psi_{J,D} + \Psi_J P_{\Gamma_J} \right)$.*

The FE method outlined in this section is equivalent to applying a standard FE method on the entire fracture network, under the assumption that the global nodes present on a given fracture intersection correspond to local nodes on both of the intersecting fractures. The advantage of the proposed FE approach over the standard FE method is two–fold: firstly, the FE method outlined in this section does not require the assembly and inversion of a global stiffness matrix; instead only local problems on each individual fracture need to be computed, together with the inversion of the linear system (12). Secondly, the number of global nodes can be reduced by performing a suitable coarsening algorithm at the fracture intersections. In large scale DFNs, such as the ones considered in this article, this approach can greatly reduce the computational work needed to solve the underlying groundwater flow problem; see [8, 13] for further details.

3. Conditioning Methods

In this section we develop two numerical methods to condition fracture transmissivities in a DFN on measured pressure values: the so-called Basis Vector Conditioning Method and the Bayesian Conditioning Method. For ease of notation, from hereon we shall refer to the residual pressure as defined in (1) as simply the 'pressure'.

The general problem setting is the following: we suppose that we are given a (deterministically defined) DFN consisting of n, $n \geq 1$, fractures, each with an initial transmissivity $\tilde{T}_{f_i}$, $i = 1, \ldots, n$. Moreover, we assume that field data has been supplied which provides a set of m measurement points $\{M_i\}_{j=1}^m$ at which the pressure has been evaluated. We collect these measured pressure values in the vector $\mathbf{P}_M$. Once the finite element approximation P_h to the analytical solution P has been computed, based on employing Algorithm 2.1, we may now evaluate P_h at the corresponding measurement points. The aim of this section is then to develop appropriate conditioning algorithms which are capable of adjusting the transmissivity field $\tilde{T}_{f_i}$, $i = 1, \ldots, n$, so that the error $\|\mathbf{P}_M - \mathbf{P}_{h,M}\|_2$ is minimised, where $\| \cdot \|_2$ denotes the standard ℓ_2–norm and $\mathbf{P}_{h,M} = (P_h(M_1), \ldots, P_h(M_m))^\top$.

3.1. Basis Vector Conditioning Method. The material in this section is based on a conditioning method proposed by Cliffe and Jackson [3, 4], where an isotropic transmissivity field was conditioned on pressure measurements in a continuous porous medium. In this section, we extend this technique so that it is applicable to a DFN.

Given a DFN consisting of n fractures, with corresponding transmissivities $\tilde{T}_{f_i}$, $i = 1, \ldots, n$, we define the vector $\mathbf{X} = (X_1, \ldots, X_n)^\top$ to be equal to the values

of the logarithm of the fracture transmissivities; more precisely, $X_i = \log_{10} \tilde{T}_{f_i}$, $i = 1, \ldots, n$. The reason why we condition on the log transmissivities instead of directly on the transmissivities themselves, is that it ensures that the corresponding conditioned transmissivities are always positive. It can be shown, see [3], for example, that for the case of small variability in fracture transmissivities and small deviations of the pressure from the mean pressure field, the conditioned realisations $\mathbf{X}^C$ of $\mathbf{X}$ are given by adding the product of a suitable set of basis vectors $\mathbf{W}$ and the vector of coefficients $\delta\mathbf{P}$ to the unconditioned fracture log transmissivities $\mathbf{X}^U$, i.e.,

$$\mathbf{X}^C = \mathbf{X}^U + \mathbf{W}\,\delta\mathbf{P} \ ,$$

where the coefficients in $\delta\mathbf{P}$ are the difference between the measured pressures P_M and the calculated pressure P_h computed at the m measurement points, i.e., $\delta\mathbf{P} = \mathbf{P}_M - \mathbf{P}_{h,M}$. The matrix $\mathbf{W}$, which contains the m basis vectors associated with each of the measurement points, can be obtained by solving the system

$$(13) \qquad (\mathbf{LCL}^\top)\mathbf{W}^\top = \mathbf{LC} \ ,$$

cf. [3]. The matrix $\mathbf{L}$ is known as the sensitivity matrix, while the covariance matrix $\mathbf{C}$ represents the correlation of the fracture transmissivities in the DFN. It is assumed that the sensitivity matrix $\mathbf{L}$ contains pressure measurements only; it represents the linear relationship between the values of $\mathbf{X}$ on the n fractures and the m measured values of pressure for small variability and small deviations of pressure from the mean pressure field. The entries of $\mathbf{L} = \{L_{ij}\}$, $i = 1, \ldots, m$, $j = 1, \ldots, n$, are thus defined as

$$(14) \qquad L_{ij} = \frac{\partial P_B(M_i)}{\partial X_j}, \qquad i = 1, \ldots, m, \ j = 1, \ldots, n,$$

where $P_B(M_i)$, $i = 1, \ldots, m$, is the computed pressure at a borehole evaluated at the ith measurement point M_i. It is defined as

$$(15) \qquad P_B(M_i) = P_h(M_i) + \frac{Q(M_i)}{\tilde{T}_{f,M_i}\kappa},$$

where $Q(M_i)$ is the flow produced from pumping the borehole at M_i, $i = 1, \ldots, m$, $\tilde{T}_{f,M_i}$ is the transmissivity of the fracture at the measurement point, and κ is a geometrical constant dependent on the FE discretisation used. Full details on the derivation of κ can be found in Milne [13]. The consequence $\mathbf{G} = (G_1, \ldots, G_m)^\top$ is also defined at each of the m measurement points to be the difference between the calculated borehole pressure and the measured pressure $\mathbf{P}_M$, i.e., defining $\mathbf{P}_B = (P_B(M_1), \ldots, P_B(M_m))^\top$, we have

$$(16) \qquad \mathbf{G}(P_h, \mathbf{X}) = \mathbf{P}_B - \mathbf{P}_M \ .$$

There are two terms needed to calculate the entries in the sensitivity matrix (14) for the case of a DFN; indeed, for a fracture f_j, $1 \le j \le n$, we have that

$$(17) \qquad L_{ij} = \int_{f_j} \frac{1}{\rho g} \frac{\partial \tilde{T}_{f_j}}{\partial X_j} \nabla\theta \cdot \nabla P_h \, dx + \frac{\partial}{\partial X_j}\left(\frac{Q(M_i)}{\tilde{T}_{f,M_i}\kappa}\right) \ , \qquad j = 1, \ldots, n.$$

Here, the first term on the right-hand side of (17) may be rewritten as

$$(18) \qquad \int_{f_j} \frac{1}{\rho g} \frac{\partial \tilde{T}_{f_j}}{\partial X_j} \nabla\theta \cdot \nabla P_h \, dx = \int_{f_j} \frac{\tilde{T}_{f_j} \log_e 10}{\rho g} \nabla\theta \cdot \nabla P_h \, dx \ ,$$

where ∇P_h is the gradient of the pressure on the fracture, f_j, $j = 1, \ldots, n$, ρ is the groundwater density, g is the gravitational acceleration and $\nabla\theta$ is the gradient of

an associated adjoint solution on the fracture. The adjoint solution is derived in Milne [13]; it is defined at global nodes as follows

$$\left(\theta^{\top}\right)_{ir} = \frac{\partial G_i}{\partial P_{\Gamma_r}} \left(\frac{\partial \Phi_s}{\partial P_{\Gamma_r}}\right)^{-1}, \qquad i = 1, \ldots, m, \ r, s = 1, \ldots, n_{\Gamma},$$

where n_{Γ} is the number of global nodes in the DFN at which the pressure P_{Γ} on a fracture intersection is calculated and $\boldsymbol{\Phi}_s$ represents the finite element equations at the fracture intersections, i.e.,

$$\boldsymbol{\Phi}_s := \begin{pmatrix} A_{11} & \cdots & A_{n_{\Gamma}1} \\ \cdots & \cdots & \cdots \\ A_{1n_{\Gamma}} & \cdots & A_{n_{\Gamma}n_{\Gamma}} \end{pmatrix} \begin{pmatrix} P_{\Gamma_1} \\ \cdots \\ P_{\Gamma_{n_{\Gamma}}} \end{pmatrix} - \begin{pmatrix} B_1 \\ \cdots \\ B_{n_{\Gamma}} \end{pmatrix} = \mathbf{0},$$

cf. (12). The adjoint solution is then calculated across the fracture network in a similar manner to the pressure (7). The second term on the right-hand side of (17) is calculated by differentiating (15) with respect to $X_j = \log_{10} \tilde{T}_{f_j}$, $j = 1, \ldots, n$, for the single fracture it corresponds to, i.e.,

$$(19) \qquad \frac{\partial}{\partial X_j} \left(\frac{Q(M_i)}{\tilde{T}_{f,M_i}\kappa}\right) = -\frac{Q(M_i)\delta_{ij}\log_{10} e}{\tilde{T}_{f_j}\kappa} ,$$

where δ_{ij} denotes the Kronecker delta function. The integral in (18) can be calculated using a numerical quadrature technique while (19) is easily evaluated. Details on the derivation of the sensitivity terms can be found in Milne [13].

The case of large variability of fracture transmissivities and large deviations of the pressure from the mean pressure field is now considered. The unconditioned log transmissivity values and basis vectors $\mathbf{W}$ are computed as before. The log of the unconditioned fracture transmissivities is denoted by $\mathbf{X}^U$ and an update to the log transmissivities is evaluated assuming the following relationship [3]

$$(20) \qquad \mathbf{X} = \mathbf{X}^U + \sum_{i=1}^{m} \alpha_i \mathbf{W}_i ,$$

where $\mathbf{W}_i$, $i = 1, \ldots, m$, denotes the ith column of the matrix $\mathbf{W}$ and α_i, $i = 1, \ldots, m$, are coefficients that are to be determined. Initially, the values of α_i, $i = 1, \ldots, m$, are set equal to zero. The coefficients α_i, $i = 1, \ldots, m$, are chosen so that they minimise an error function $E(\alpha)$ defined as the weighted sum of consequences defined in (16), namely,

$$(21) \qquad E(\alpha) = \sum_{i=1}^{N} \frac{G_i^2}{\sigma_i^2} ,$$

where σ_i is a weight corresponding to the estimated experimental error in the measurement of the pressure at measurement point M_i, $i = 1, \ldots, m$. Our fracture network model depends non-linearly on α_i, $i = 1, \ldots, m$, thereby minimisation of (21) will proceed in an iterative manner. There are many different algorithms for non-linear minimisation and the Levenberg-Marquardt method [16] is exploited to efficiently minimise $E(\alpha)$. The Levenberg-Marquardt algorithm requires the derivative

$$(22) \qquad \beta_k = \frac{\partial E}{\partial \alpha_k} = \sum_{i=1}^{m} \frac{2G_i}{\sigma_i^2} \frac{\partial G_i}{\partial \alpha_k}, \qquad k = 1, \ldots, m ,$$

and

$$\text{(23)} \qquad \gamma_{kl} = \frac{\partial^2 E}{\partial \alpha_k \partial \alpha_l} \approx \sum_{i=1}^{m} \frac{2}{\sigma_i^2} \left[\frac{\partial G_i}{\partial \alpha_k} \frac{\partial G_i}{\partial \alpha_l} \right], \qquad l, k = 1, \ldots, m \ ;$$

here, for simplicity of implementation, the second derivative of G_i, $i = 1, \ldots, n$, has been neglected. The term $\partial G_i / \partial \alpha_k$ can be calculated using the chain rule with the sensitivity values. The increments of the coefficients $\delta \alpha$ are calculated by solving the system

$$\text{(24)} \qquad \sum_{l=1}^{m} \acute{\gamma}_{kl} \delta \alpha_l = \beta_k, \qquad k = 1, \ldots, m \ ,$$

where

$$\acute{\gamma}_{jk} = \begin{cases} \gamma_{jk}(1 + \lambda) \ , & j = k \ , \\ \gamma_{jk} \ , & j \neq k \ , \end{cases}$$

and λ is a parameter initially set to a small value which is adaptively updated at each iteration. Here, λ controls whether the Levenberg-Marquardt method corresponds to a steepest descent method or a Newton method for the minimisation at each iteration.

The overall minimisation algorithm is summarised as follows.

Algorithm 3.1. *Basis Vector Conditioning Algorithm*
  (1) *Compute the initial log transmissivity field $\mathbf{X}^U$ and calculate an initial error from (21).*
  (2) *Calculate the sensitivities using (18) and (19).*
  (3) *Calculate the basis vectors $\mathbf{W}$ using (13).*
  (4) *Select an initial guess for the coefficients α.*
  (5) *Update $\mathbf{X}$ using (20).*
  (6) *Re-calculate pressures with the new $\mathbf{X}$ value.*
  (7) *Update the new derivatives β (22) and γ (23).*
  (8) *Calculate new increment for the coefficients $\delta \alpha$ from (24).*
  (9) *If the error (21) has converged then stop. If the error has not been reduced then increase λ by a factor of 10 and return to step 6. If the error has been reduced then decrease λ by a factor of 10 and update $X(\alpha)$ to $X(\alpha + \delta \alpha)$ and return to step 6.*

3.2. Bayesian Conditioning Method. The vector of fracture log transmissivities is denoted by $\mathbf{X}$ and $\mathbf{m}$ denotes the vector of mean fracture log transmissivities. $\mathbf{X}$ is assumed to have a prior Gaussian distribution, defined as

$$\text{(25)} \qquad f(\mathbf{X}) = \mathbf{A}_1 \exp \left\{ -\frac{1}{2} (\mathbf{X} - \mathbf{m})^\top \mathbf{C}^{-1} (\mathbf{X} - \mathbf{m}) \right\} \ ,$$

where the matrix $\mathbf{C}$ is the covariance matrix of the fracture log transmissivities $\mathbf{X}$, which may or may not be correlated, and $\mathbf{A}_1$ is a constant vector. The pressures $\mathbf{P}_{h,M}$ calculated at measurement points are a function of the fracture log transmissivities, i.e.,

$$\mathbf{P}_{h,M} = \mathbf{P}_{h,M}(\mathbf{X}).$$

Furthermore, the measured pressures are assumed to be known to within some measurement error ε and it is assumed that they are independent, normally distributed random variables with possibly different standard deviations for each measurement. Accordingly, the measured pressures $\mathbf{P}_M$ are equal to the sum of the mean values of the measured pressures $\bar{\mathbf{P}}_M$ and a vector of measurement errors ε, i.e.,

$$\text{(26)} \qquad \mathbf{P}_M = \bar{\mathbf{P}}_M + \varepsilon \ .$$

Bayes' Theorem can be used to write down the posterior distribution for $\mathbf{X}$ defined as

$$(27) \qquad f(\mathbf{X}|\mathbf{P}_M) = \frac{f(\mathbf{P}_M|\mathbf{X}) f(X)}{f(\mathbf{P}_M)} .$$

The term $f(\mathbf{X})$ is the prior distribution of fracture log transmissivities defined in (25), while the term $f(\mathbf{P}_M|\mathbf{X})$ takes into account the measured pressure values and is given by

$$(28) \qquad f(\mathbf{P}_M|\mathbf{X}) = \mathbf{A}_2 \exp\left\{-\frac{1}{2}(\mathbf{P}_{h,M} - \mathbf{P}_M)^\top \mathbf{\Sigma}^{-1}(\mathbf{P}_{h,M} - \mathbf{P}_M)\right\} ,$$

where $\mathbf{A}_2$ is a constant vector, the matrix $\mathbf{\Sigma}$ is the covariance matrix of the error ε in the measured pressures; thus $\mathbf{\Sigma}$ will be a diagonal matrix if the measured pressures are independent. The normalisation constant $f(\mathbf{P}_M)$ is unknown, but using (25), (27) and (28) we can state

$$(29)
\begin{aligned}
f(\mathbf{X}|\mathbf{P}_M) &\propto \exp\left\{-\frac{1}{2}(\mathbf{X} - \mathbf{m})^\top \mathbf{C}^{-1}(\mathbf{X} - \mathbf{m})\right\} \\
&\quad \times \exp\left\{-\frac{1}{2}(\mathbf{P}_{h,M} - \mathbf{P}_M)^\top \mathbf{\Sigma}^{-1}(\mathbf{P}_{h,M} - \mathbf{P}_M)\right\} .
\end{aligned}$$

Equation (29) can be used to compute the posterior mode for $\mathbf{X}$, where $f(\mathbf{X}|\mathbf{P}_M)$ is at a maximum and can be found by solving $\frac{df(\mathbf{X}|\mathbf{P}_M)}{d\mathbf{X}} = \mathbf{0}$. This finds the most probable set of fracture log transmissivities that yield the given measured pressures. The exponential function is monotonic so it is also true that the posterior mode for $\mathbf{X}$ occurs when $\frac{d}{d\mathbf{X}}\{\ln f(\mathbf{X}|\mathbf{P}_M)\} = \mathbf{0}$ and it follows that

$$(30)
\begin{aligned}
\frac{d}{d\mathbf{X}} \Bigg\{ -\Bigg[&\left(\frac{1}{2}(\mathbf{X} - \mathbf{m})^\top \mathbf{C}^{-1}(\mathbf{X} - \mathbf{m})\right) \\
&+ \left(\frac{1}{2}(\mathbf{P}_{h,M} - \mathbf{P}_M)^\top \mathbf{\Sigma}^{-1}(\mathbf{P}_{h,M} - \mathbf{P}_M)\right) \Bigg] \Bigg\} = \mathbf{0} .
\end{aligned}$$

Applying the product rule for vectors to (30), the mode of the posterior distribution $f(\mathbf{X}|\mathbf{P}_M)$ can be found when

$$(31) \quad \mathbf{F}(\mathbf{X}) \equiv (\mathbf{X} - \mathbf{m})^\top (\mathbf{C}^{-1} + \mathbf{C}^{-\top}) + (\mathbf{P}_{h,M} - \mathbf{P}_M)^\top (\mathbf{\Sigma}^{-1} + \mathbf{\Sigma}^{-\top})\frac{d\mathbf{P}_{h,M}}{d\mathbf{X}} = \mathbf{0} .$$

Equation (31) can be solved using the Newton method to compute the posterior mode of $\mathbf{X}$. The Newton method generates a sequence for updating the log transmissivities $\mathbf{X}_k$ at the kth iteration by the recurrence formula

$$\mathbf{X}_{k+1} = \mathbf{X}_k + \mathbf{d}_k ,$$

where $\mathbf{d}_k$ solves (31) linearised at $\mathbf{X}_k$, i.e., $\mathbf{d}_k$ satisfies

$$\mathbf{F}(\mathbf{X}_k) + \frac{d\mathbf{F}_k}{d\mathbf{X}_k}\mathbf{d}_k = \mathbf{0} ,$$

and so if $\frac{d\mathbf{F}_k}{d\mathbf{X}_k}$ is non-singular

$$\mathbf{d}_k = -\left(\frac{d\mathbf{F}_k}{d\mathbf{X}_k}\right)^{-1} \mathbf{F}(\mathbf{X}_k) .$$

Now,

$$(32) \qquad \frac{d\mathbf{F}_k}{d\mathbf{X}_k} = (\mathbf{C}^{-1} + \mathbf{C}^{-\top}) + \left(\frac{d\mathbf{P}_{h,M}}{d\mathbf{X}_k}\right)^{\top} \mathbf{\Sigma}^{-1} \frac{d\mathbf{P}_{h,M}}{d\mathbf{X}_k}$$
$$+ (\mathbf{P}_{h,M}(\mathbf{X}_k) - \mathbf{P}_M)^{\top} (\mathbf{\Sigma}^{-1} + \mathbf{\Sigma}^{-\top}) \frac{d^2 \mathbf{P}_{h,M}}{d\mathbf{X}_k^2} \ .$$

In minimisation problems such as ours it is common to drop the term $\frac{d^2 \mathbf{P}_{h,M}}{d\mathbf{X}_k^2}$ from (32), cf. [16]. Thus, from hereon we use the approximation

$$(33) \qquad \frac{d\mathbf{F}_k}{d\mathbf{X}_k} \approx (\mathbf{C}^{-1} + \mathbf{C}^{-\top}) + \left(\frac{d\mathbf{P}_{h,M}}{d\mathbf{X}_k}\right)^{\top} \mathbf{\Sigma}^{-1} \frac{d\mathbf{P}_{h,M}}{d\mathbf{X}_k} \ .$$

The algorithm to condition fracture log transmissivities $\mathbf{X}$ on pressure measurements $\mathbf{P}_M$ is now summarised in Algorithm 3.2.

Algorithm 3.2. *Bayesian Conditioning Algorithm*
  (1) *Take the initial set of fracture log transmissivities $\mathbf{X}_0 = \mathbf{m}$ and set $k = 0$.*
  (2) *Compute $\mathbf{F}(\mathbf{X}_k)$ and $\frac{d\mathbf{F}_k}{d\mathbf{X}_k}$.*
  (3) *Compute the increment $\mathbf{d}_k$ from the system $\left(\frac{d\mathbf{F}_k}{d\mathbf{X}_k}\right) \mathbf{d}_k = -\mathbf{F}(\mathbf{X}_k)$.*
  (4) *Update the fracture log transmissivities $\mathbf{X}_{k+1} = \mathbf{X}_k + \mathbf{d}_k$.*
  (5) *Calculate the new pressures $\mathbf{P}_{h,M}(\mathbf{X}_{k+1})$*
  (6) *Update the sensitivities $\frac{d\mathbf{P}_{h,M}(\mathbf{X}_{k+1})}{d\mathbf{X}_{k+1}}$.*
  (7) *If the convergence criteria has been met then stop. Otherwise set $k = k+1$ and return to step 2.*

4. Test Cases

In this section we outline two DFN models which are used as test cases. The first test case comprises of 501 fracture transmissivities to be conditioned on nine measured pressures obtained at boreholes. The second test case contains two large macro fractures tessellated (divided into smaller sub fractures) into 900 sub-fractures each. This second test case is divided into two subcases: Test case 2a is used to model the two macro fractures, while Test case 2b consists of the two macro fractures, together with a background fracture population of 24926 smaller sized fractures.

For the two test cases under consideration, we assume that the transmissivity is constant on each individual fracture (or subfracture tessellation, in the case of test case 2). Moreover, we point out that the unconditioned pressure values calculated on both DFN test cases fail to match the measured pressures at the measurement points.

4.1. Test Case 1. This test case is a DFN model of a potential site for nuclear waste disposal in Finland. It is planned to construct a repository in the centre of an island called Olkiluoto which lies in the Baltic sea and is approximately 10 km^2 in size. The site has been characterised through various surface and subsurface measurements [7]. Boreholes have been drilled at locations spread across the site, which provide pressure measurements at given depths. Pumping tests undertaken on boreholes give an idea of approximate transmissivity properties of fracture zones located between the drilled boreholes.

The Olkiluoto site data [7] was implemented in ConnectFlow to produce a DFN model of the site containing 11 fracture sets that were generated based on pumping test results, and on fracture orientation and length estimates and ranges [6]. Each
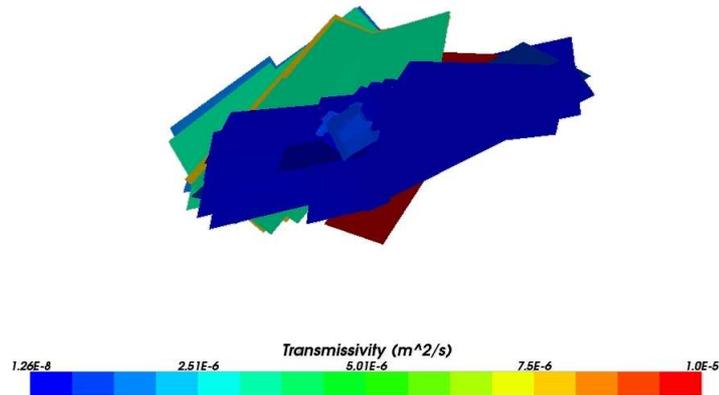
FIGURE 1. Test Case 1: DFN containing 11 fracture sets coloured by fracture transmissivity and 9 borehole measurement points shown as purple dots; a total of 501 fractures make up the entire network.

fracture set contains fractures with similar geometry and a total of 501 fractures are contained in the different fracture sets. The domain of the model containing these fracture sets is 7800m by 7800m by 1000m. The fracture set transmissivities were assumed to be homogeneous; that is all initial fracture transmissivities contained in the same fracture zone are equal. Measured pressure values were obtained at measurement points at nine boreholes. The boundary conditions of the model are as follows: the top surface has pressure proportional to elevation; the lateral sides which are in contact with the Baltic Sea have pressure set to zero; and the bottom surface has a no-flow boundary condition. Figure 1 shows the location of the borehole measurement points and the geometry of the 501 fractures coloured according to their transmissivity value.

The model has been simplified by only modelling borehole measurement points instead of including complete boreholes which would further connect some of the fractures.

4.2. Test Case 2. This test case focuses on a smaller area of the Olkiluoto site than that modelled by test case 1. The problem domain is a 300m by 300m by 500m cube approximately centred around nine boreholes located in the middle of the Olkiluoto island. It should be noted that these boreholes do not correspond to those used in test case 1. This scenario was designed to analyse a series of cross-hole pump tests with the nine boreholes, where one borehole is pumped with a given flow rate and the responses of the remaining boreholes are recorded as measured pressures.

The geometry of the DFN is semi-deterministic; it contains two large scale tessellated macro fractures which are known to provide flow paths through the domain. Additionally, there is a background fracture population consisting of many smaller
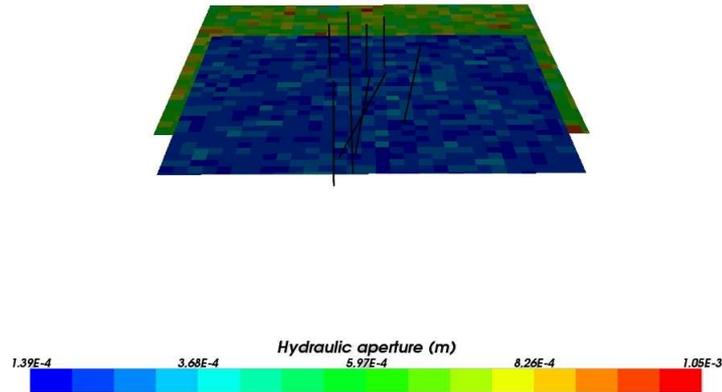
FIGURE 2. Test Case 2a: Domain of test case 2a with two tessellated macro fractures (macro fracture 1 and 2) intersected by nine boreholes. Macro fracture 1 is mainly green coloured with macro fracture 2 mainly blue coloured.

fractures throughout the domain. To study the effect of the background population, test case 2 has been split into two separate test cases. The same value of measured pressures and measurement locations were used to condition the fracture transmissivities in both of these test cases.

4.2.1. Test Case 2a. Test case 2a contains the two macro fractures, each tessellated into 900 sub-fractures. Here, zero pressure boundary conditions are used on all the boundaries of the domain. The two macro fractures are shown in Figure 2 with the hydraulic aperture (which is proportional to the cube of the fracture transmissivity) shown, as this shows the fracture tessellation more clearly. Macro fracture 1 and macro fracture 2 have mean transmissivities estimated from field experiments of 2.2E-4m^2/s and 1.0E-5m^2/s, respectively. The initial fracture apertures were generated by sampling from a normal distribution using corresponding aperture means to the transmissivity means. The initial transmissivities of the sub-fractures on each macro fracture were then assigned by converting the fracture apertures to fracture transmissivities using the cubic law [21].

The sub-fractures were assumed to be exponentially correlated. Defining the separation S_{ij} of two sub-fractures i and j as the distance between the centre of sub-fracture i and the centre of sub-fracture j, the standard deviation of sub-fracture log transmissivities as σ_X (assumed to be constant for all sub-fractures on the same macro fracture) and the correlation scale as ap, then the covariance matrix C_k of the sub-fractures transmissivities on macro fracture k is defined as

$$(34) \qquad C_k(i,j) = \begin{cases} \sigma_X^2, & i = j \ , \\ \sigma_X^2 \exp\left\{\frac{-S_{ij}}{ap}\right\}, & i \neq j \ . \end{cases}$$
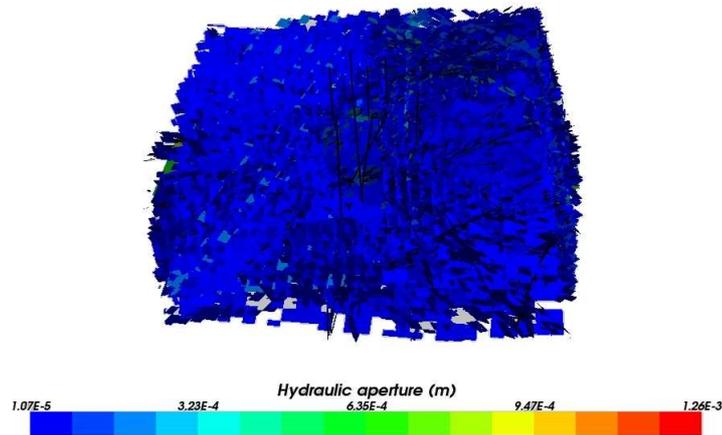
FIGURE 3. Test Case 2b: Domain of test case 2b with two tessellated macro fractures intersected by nine boreholes and the addition of a background fracture population.

4.2.2. Test Case 2b. In addition to the two tessellated macro fractures, a background fracture population was added into the model domain providing additional flow paths between the two macro fractures and the boreholes contained in the model. A total of 24926 background fractures were included, whose statistical properties were derived from borehole orientation and location data. The main unknown of the background fracture population was the fracture size which was chosen so that the background fractures were large enough to make a well connected system between the macro fractures and the domain boundaries. The model domain is shown in Figure 3.

5. Results

In this section, we now present computational results to highlight the performance of the conditioning methods outlined in Section 3. Here, in addition to computing the (absolute) error $\|\mathbf{P}_M - \mathbf{P}_{h,M}\|_2$ between the measured pressure values, and those computed using each of the above conditioning algorithms, we shall also compute the following relative error:

$$\|\mathbf{P}_M - \mathbf{P}_{h,M}\|_R = \frac{1}{m}\sum_{i=1}^{m}\frac{|(P_M)_i - P_h(M_i)|}{(P_M)_i}.$$

5.1. Test Case 1 Results. In this section, we assume that the fracture transmissivities are uncorrelated and accordingly set the covariance matrix $\mathbf{C}$ equal to the $(n \times n)$ identity matrix $\mathbf{I}_n$.

5.1.1. Basis Vector Conditioning Results. In this section, we first consider the application of the basis vector conditioning method to Test Case 1. To this end, Figure 4 compares the conditioned pressure to both the measured pressure and the initial unconditioned pressures at all nine measurement points in test case 1. It can be seen that the conditioned pressures give a closer match to the measured
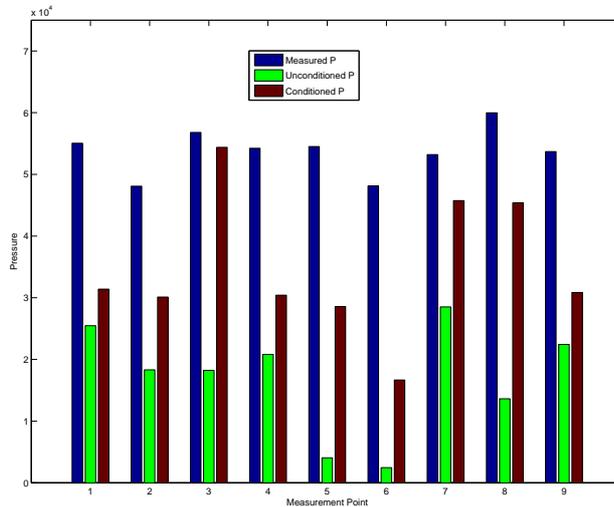
FIGURE 4. Test Case 1. The measured pressures, unconditioned pressures and conditioned pressures at the nine measurement points using the basis vector conditioning algorithm.

	$\|\mathbf{P}_M - \mathbf{P}_{h,M}\|_2$	$\|\mathbf{P}_M - \mathbf{P}_{h,M}\|_R$
Initial	1.1128E+5	0.6828
Final	6.2327E+4	0.3574

TABLE 1. Test Case 1: Initial and final absolute and relative errors using the basis vector conditioning algorithm.

pressures at every measurement point compared to the unconditioned pressures, though an exact match is not achieved. In Table 1 we compute the initial and final absolute and relative errors between the calculated pressures and the measured pressure values. Here, we clearly observe that the basis vector conditioning algorithm yields a significant improvement in the computed pressure values when compared to the initial (unconditioned) solution. Indeed, norms of the error are approximately half of their initial values. It is clear that, while the conditioned pressures give a far better match to the measured pressures than the unconditioned pressures, the match is perhaps not as close as one would like; indeed, the final relative error is still around 36%, which is quite high. With this in mind, we now proceed to apply the Bayesian algorithm to this test case.

5.1.2. Bayesian Conditioning Results. For all of the Bayesian conditioning results presented in this article, we assume that each pressure measurement is independent and that all measurements have the same standard deviation σ_P in the measured pressure. Thus, the covariance matrix $\mathbf{\Sigma}$ from (31) takes the form

$$\mathbf{\Sigma} = \sigma_P^2 \mathbf{I}_m \ ,$$

where $\mathbf{I}_m$ is the $m \times m$ identity matrix and the variance σ_P^2 at a pressure measurement point M_i, $i = 1, \ldots, m$, is defined as

$$\sigma_P^2 = C((P_M)_i, (\bar{P}_M)_i) = E(((P_M)_i - (\bar{P}_M)_i)((P_M)_i - (\bar{P}_M)_i)) \ ,$$
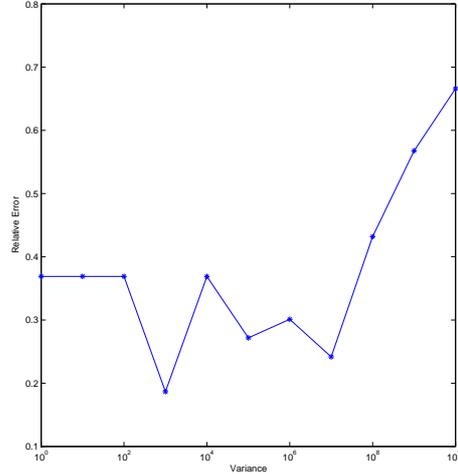
FIGURE 5. Test Case 1: Variance σ_P^2 of the pressure measurements against the relative error using the Bayesian conditioning algorithm.

where $C(\cdot, \cdot)$ denotes the covariance, $E(\cdot)$ denotes the expectation and $\bar{P}_M$ denotes the mean value of the measured pressure. In Figure 5, we plot the relative error against the variance of the pressure measurements σ_P^2. It can be seen that the relative error possesses a minimum when the variance in the pressure measurements is $\sigma_P^2 = 1.0E+3$; indeed, here $\|\mathbf{P}_M - \mathbf{P}_{h,M}\|_R = 0.1866$. We recall, that this is around half the relative error achieved when the basis vector conditioning method is employed, cf. Section 5.1.1. However, as the variance in the pressure measurements σ_P^2 increases beyond a value of 1.0E+8, we observe that the relative error starts to increase. This represents the point at which the standard deviation of the pressure measurements is of the same magnitude as the pressure measurements themselves ($\sigma_P = 1.0E+4$).

In order to improve the match to measured pressures even further, we consider the following algorithm outlined below, which is based on adaptively selecting the variance in the pressure measurements.

Algorithm 5.1. *Updating the Variance.*
(1) *Set the initial fracture log transmissivities values $\mathbf{X} = \mathbf{X}_0$ and set $i = 0$.*
(2) *Run the Bayesian conditioning algorithm for step i on the fracture log transmissivities $\mathbf{X}$ with variance σ_P^2 of the pressure measurements ranging from 1.0E+0 to 1.0E+10.*
(3) *Take the conditioned log transmissivity values $\mathbf{X}^C$ that correspond to the variance value σ_P^2 with the smallest final absolute error as the new initial fracture transmissivities. That is set $\mathbf{X} = \mathbf{X}^C$*
(4) *If the absolute error is below a given tolerance then stop. Otherwise, set $i = i + 1$ and go to (2).*

In Figure 6 we plot the variance σ_P^2 in the measured pressure values against the relative error for each step in Algorithm 5.1. Each point represents one run of the Bayesian conditioning algorithm. Here, we observe that as the algorithm proceeds, the relative error in the computed pressures becomes relatively insensitive to the
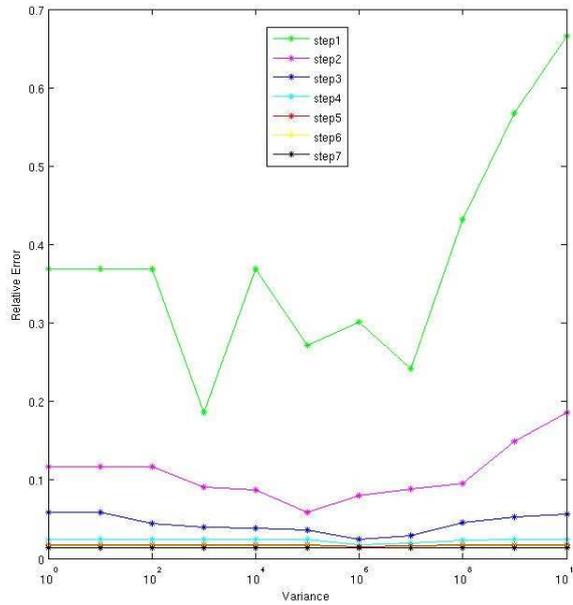
FIGURE 6. Test Case 1: Variance σ_P^2 of the pressure measurements against the relative error for each iteration (step) of Algorithm 5.1.

Step	$\|\mathbf{P}_M - \mathbf{P}_{h,M}\|_2$	$\|\mathbf{P}_M - \mathbf{P}_{h,M}\|_R$
Unconditioned	1.1128E+5	0.6828
1	4.1522E+4	0.1866
2	1.4791E+4	0.0587
3	5.6679E+3	0.0243
4	4.7318E+3	0.0175
5	4.5264E+3	0.0158
6	4.3127E+3	0.0141
7	4.2446E+3	0.0133

TABLE 2. Test Case 1: Minimum absolute and relative errors at each step of Algorithm 5.1.

specified value of the variance σ_P^2 in the measured pressure values. Indeed, from steps 4 onwards, the curves are essentially horizontal. Table 2 presents a summary of the minimum absolute and relative errors at each step of Algorithm 5.1. Here, we observe that both the absolute and relative errors converge to a relatively constant value after the first 4 steps of Algorithm 5.1 have been computed. In Figure 7 we compare the conditioned pressures computed from step 7 of Algorithm 5.1 to the unconditioned and measured pressures. Here, we clearly observe the excellent match that has been attained based on employing Algorithm 5.1. Indeed, with the exception of the third and sixth measurement points, the measured pressure is almost identically matched at the other seven measurement points.

Finally, in Table 3 we compare the final absolute and relative errors of the two newly proposed conditioning methods applied to test case 1. As already noted,
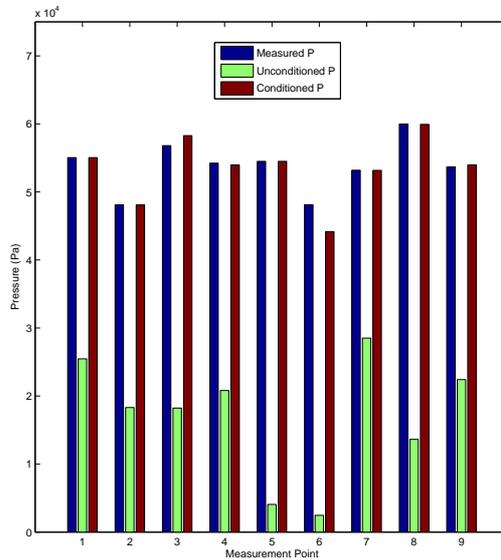
FIGURE 7. Test Case 1: The measured pressure, unconditioned pressure and conditioned pressure from Algorithm 5.1 at each measurement point.

Method	$\|\mathbf{P}_M - \mathbf{P}_{h,M}\|_R$	$\|\mathbf{P}_M - \mathbf{P}_{h,M}\|_R$
Unconditioned	1.1128E+5	0.6828
Basis vector	6.2327E+4	0.3574
Algorithm 5.1	4.2446E+3	0.0133

TABLE 3. Test Case 1: Final absolute and relative errors for the conditioning methods.

we observe that Algorithm 5.1 produces the smallest absolute and relative errors. Indeed, the relative error from Algorithm 5.1 is more than 26 times smaller than that from the basis vector conditioning method and 51 times smaller than the unconditioned relative error.

5.2. Test Case 2 Results. On the basis of the computations undertaken for test case 1, we only consider the application of the Bayesian conditioning method based on Algorithm 5.1 to condition the fracture transmissivities in test case 2.

5.2.1. Test Case 2a Results. In this section we set $\sigma_X = 1/6$ and $ap = 5$ in order to construct the fracture log transmissivity covariance matrix $\mathbf{C}$ defined in (34). As for the previous example, in Figure 8 we plot the relative error against the variance in the pressure measurements for each step of Algorithm 5.1. As previously observed, we see that as the algorithm proceeds, the relative error in the computed pressures becomes relatively insensitive to the specified value of the variance σ_P^2 in the measured pressure values. However, in this setting we notice that while the curves become flatter as the algorithm proceeds, there is still a visible growth in $\|\mathbf{P}_M - \mathbf{P}_{h,M}\|_R$ as the variance is increased. A summary of the minimum absolute and corresponding relative errors at each step of Algorithm
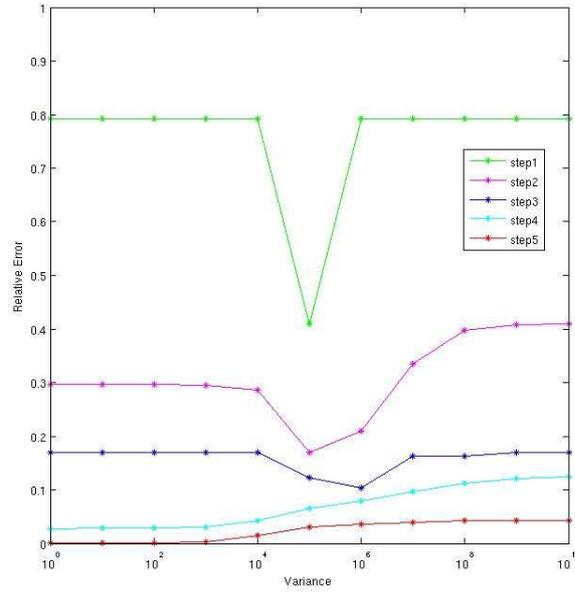
FIGURE 8. Test Case 2a: Plot of the relative error against variance in the pressure measurements for each step of Algorithm 5.1.
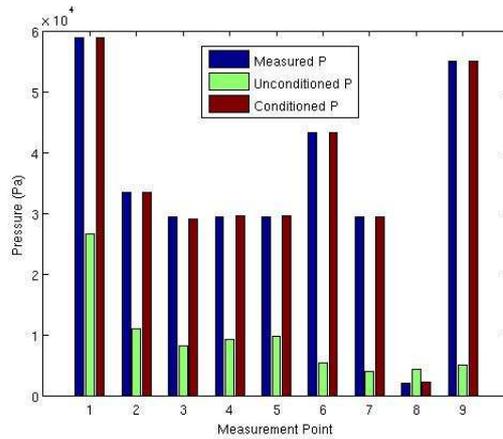

FIGURE 9. Test Case 2a: Conditioned pressures after step 5 of Algorithm 5.1 at each measurement point compared to the measured and unconditioned pressure values.

5.1 are shown in Table 4 for this test case. Here, we now observe that after 5 steps of Algorithm 5.1, the conditioned pressures provide an excellent match to the measured pressures. Indeed, this is clearly visible in Figure 9, where we plot the final conditioned pressures after step 5 of Algorithm 5.1, together with the unconditioned and measured values at each measurement point.

Step	$\|\mathbf{P}_M - \mathbf{P}_{h,M}\|_2$	$\|\mathbf{P}_M - \mathbf{P}_{h,M}\|_R$
Unconditioned	8.5860E+4	0.7929
1	3.8363E+4	0.4094
2	1.3904E+4	0.1695
3	7.9760E+3	0.1242
4	1.9890E+3	0.0429
5	8.1150E+1	0.0007

TABLE 4. Test Case 2a: Minimum absolute and relative errors at each step of Algorithm 5.1.

Step	$\|\mathbf{P}_M - \mathbf{P}_{h,M}\|_2$	$\|\mathbf{P}_M - \mathbf{P}_{h,M}\|_R$
Unconditioned	8.9737E+4	0.7984
1	4.0773E+4	1.0812
2	1.5625E+4	0.7318
3	4.1325E+3	0.0960
4	1.6182E+2	0.0048

TABLE 5. Test Case 2b: Minimum absolute and relative errors at each step of Algorithm 5.1.

5.2.2. Test Case 2b Results. This final test case involves a total of 26727 fracture transmissivities which need to be conditioned. Given the size of this problem, it was computationally too expensive to run the Bayesian conditioning algorithm to condition every fracture transmissivity. Instead, fractures to be conditioned were selected depending on their sensitivity values. To this end, fractures that had a sensitivity value of 1.0 or greater with respect to any of the measured pressures were selected for conditioning. This resulted in 2205 fracture transmissivities (with the greatest sensitivity values) being conditioned, while leaving the remaining fracture transmissivities constant at their initial value throughout the Bayesian conditioning algorithm. In other words, only selected fracture transmissivities were conditioned but pressure values were re-calculated using all of the fracture transmissivities in the DFN (including those held constant). Furthermore, due to the computational time taken to perform the conditioning of fracture transmissivities, the values of σ_P^2 in each step of Algorithm 5.1 were limited to 1.0E+3, 1.0E+4, 1.0E+5, and 1.0E+6. This selection was based on results from the previous test cases where no values of σ_P^2 less than 1.0E+3 or greater than 1.0E+6 minimised the absolute error at any step of Algorithm 5.1.

In Table 5 we show the minimum absolute and relative errors for each step of Algorithm 5.1 for test case 2b. The relative error at steps 1 and 2 are higher than would be expected compared to the previous test cases. This was due to the small measured pressure value at measurement point 8. At steps 1 and 2 the conditioned pressure at measurement point 8 was considerably higher than the measured pressure which greatly affected the value of $\|\mathbf{P}_M - \mathbf{P}_{h,M}\|_R$. Notwithstanding this issue, we see that after 4 steps of Algorithm 5.1, the relative error is less than 0.5%. Indeed, Figure 10 clearly highlights the excellent match with the measured pressures attained by the conditioned pressures. For completeness, in Figure 11 we plot the absolute error against the variance in the pressure measurements for each step of Algorithm 5.1; the absolute error was chosen, rather than the relative error, due to the issue with measurement point 8 outlined above.
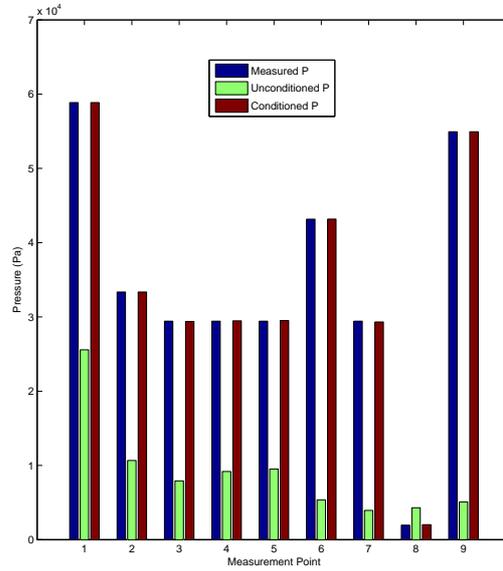
FIGURE 10. Test Case 2b: Conditioned pressures after step 4 of Algorithm 5.1 at each measurement point compared to the measured and unconditioned pressure values.
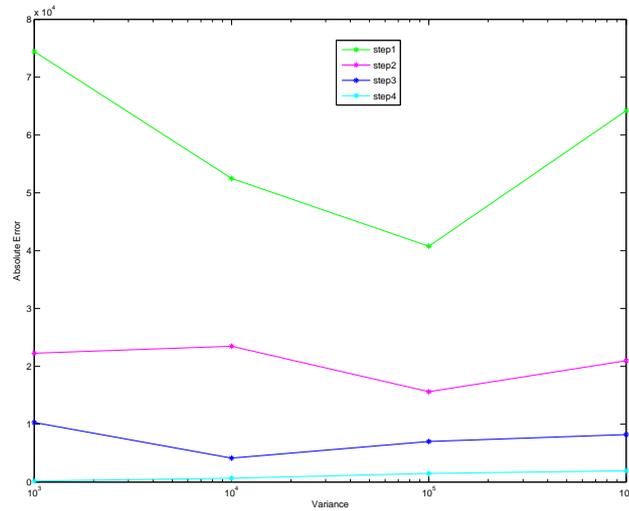

FIGURE 11. Test Case 2b: Plot of the absolute error against variance in the pressure measurements for each step of Algorithm 5.1.

6. Summary and Conclusion

In this article, we have presented two new conditioning methods which are capable of conditioning fracture transmissivities in a DFN on measured pressure values.

The first approach is based on the computation of suitable basis vectors, together with the solution of a nonlinear optimisation problem. This method represents the extension of the work, undertaken by Cliffe and Jackson [3, 4] in the context of continuous porous media problems, to DFNs. The second approach outlined is a Bayesian conditioning method that calculates a mode (point of highest likelihood for the fracture transmissivities given the measured pressures) of the posterior distribution of the fracture transmissivities numerically. Both methods have been numerically tested on a potential site for nuclear waste disposal at the Olkiluoto site in Finland. While both conditioning methods improved the match of the computed pressures to the measured experimental values, the Bayesian approach was seen to be superior, in the sense that it gave rise to the smallest relative error between the measured and conditioned pressures, evaluated at the measurement points. This method was further tested on a smaller area of the Olkiluoto site. In this setting, we considered two cases: firstly, when the DFN consists of only two large tessellated fractures, and secondly, when these two large tessellated fractures are supplemented by a background fracture population. In both cases, the Bayesian conditioning method provided an excellent match to the measured pressure values.

References

[1] J. Bear. *Dynamics of Fluids in Porous Media*. Elsevier, New York, 1972.

[2] J. Carrera and S. P. Neuman. Estimation of aquifer parameters under transient and steady state conditions: 1. Maximum liklihood method incorporating prior information. *Water Resour. Res.*, 22(2):199–210, 1986.

[3] K.A. Cliffe and C.P. Jackson. Conditioning stochastic groundwater flow models on head data. In *Materials Research Society Symposium Proceedings*, volume 353, page 7, 1995.

[4] K.A. Cliffe and C.P. Jackson. A new method for conditioning stochastic groundwater flow models on head data. Technical report, Harwell, AEA Technology, 2000.

[5] A. Frampton and V. Cvetkovic. Inference of field-scale fracture transmissivities in crystalline rock using flow log measurements. *Water Resour. Res.*, 46:W11502, 2010.

[6] A. Frampton, V. Cvetkovic, and D. Holton. Aspo task force on modeling of groundwater flow and transport of solutes - Task 7A, Task 7A1 and 7A2: Reduction of performance assessment uncertainty through modeling of hydraulic tests at Olkiluoto, Finland. Technical report, 2008.

[7] L. Koskinen H. Ahokas. Task 7: Modelling the KR24 long-term pumping test at Olkiluoto. Technical report, 2005.

[8] L. Hartley. NAPSAC release 9.3 technical summary document. Technical report, Serco Assurance, 2000.

[9] M.C. Hill and C.R. Tiedeman. *Effective Groundwater Model Calibration*. John Wiley & Sons, 2007.

[10] L. Jing. A review of techniques, advances and outstanding issues in numerical modelling for rock mechanics and rock engineering. *Int. J. Rock Mech. Min.*, 40:283–353, 2003.

[11] P.K. Kitanidis. On the geostatistical approach to the inverse problem. *Adv. Water Resour.*, 19(6), 1996.

[12] R. Marrett. Aggregate properties of fracture populations. *J. Struct. Geol.*, 18(2/3):9, 1996.

[13] A. Milne. *Topics in Flow in Fractional Media*. PhD thesis, School of Mathematical Sciences, University of Nottingham, 2011.

[14] S.P. Neuman. Calibration of distributed parameter groundwater flow models viewed as a multiple-objective decision process under uncertainty. *Water Resour. Res.*, 9(4):1006–1021, 1973.

[15] S.P. Neuman, G.E. Hogg, and E.A. Jacobson. A statistical approach to the inverse problem of aquifer hydrology: 2. Case study. *Water Resour. Res.*, 16(1):33–58, 1980.

[16] W.H. Press, B.P. Flannery, S.A. Teukolsky, and W.T. Vetterling. *Numerical Recipes*. Cambridge University Press, 1986.

[17] D. T. Snow. The frequency and apertures of fractures in rock. *Int. J. Rock Mech. Min.*, 7:23–40, 1970.

[18] A.M. Stuart. Inverse problems: A Bayesian perspective. In A. Iserles, editor, *Acta Numerica*, pages 451–559. Cambridge University Press, 2010.

[19] C.R. Tiedeman, D.J. Goode, and P.A. Hsieh. Characterizing a groundwater basin in a new england mountain and valley terrain. *Ground Water*, 36(4):611620, 1998.

[20] R.M. Yager. Simulated three-dimensional groundwater flow in the lockport group, a fractures-dolomite aquifer near Niagara Falls, New York. Technical report, USGS Water Resources Investigation Report 924189, U.S. Geological Survey, Reston, Va., 1993.

[21] R.W. Zimmerman and G.S. Bodvarsson. Hydraulic conductivity of rock fractures. *Transport Porous Med.*, 23(1):1–30, 1996.

School of Mathematical Sciences, University of Nottingham, University Park, Nottingham, NG7 2RD, UK.
E-mail: `Andrew.Cliffe@nottingham.ac.uk`

Serco, Harwell, UK
E-mail: `David.Holton@serco.com`

School of Mathematical Sciences, University of Nottingham, University Park, Nottingham, NG7 2RD, UK.
E-mail: `Paul.Houston@nottingham.ac.uk`

Serco, Harwell, UK
E-mail: `CPeter.Jackson@sercoassurance.com`

Serco, Harwell, UK
E-mail: `Steve.Joyce@serco.com`

School of Mathematical Sciences, University of Nottingham, University Park, Nottingham, NG7 2RD, UK.
E-mail: `pmxam3@nottingham.ac.uk`